

# Spin-Orbital Intertwined Topological Superconductivity in a Class of Correlated Noncentrosymmetric Materials

Lichuang Wang,<sup>1,2,\*</sup> Ran Wang,<sup>1,2,\*</sup> Xinliang Huang,<sup>1,2</sup> Xianxin Wu,<sup>3,†</sup> and Ning Hao<sup>1,2,‡</sup>

<sup>1</sup>Anhui Provincial Key Laboratory of Low-Energy Quantum Materials and Devices,  
High Magnetic Field Laboratory, HFIPS, Chinese Academy of Sciences, Hefei, Anhui 230031, China

<sup>2</sup>Science Island Branch of Graduate School, University of Science and Technology of China, Hefei, Anhui 230026, China

<sup>3</sup>CAS Key Laboratory of Theoretical Physics, Institute of Theoretical Physics,  
Chinese Academy of Sciences, Beijing 100190, China

In this study, we propose an alternative route to achieving topological superconductivity (TSC). Our approach applies to a new class of correlated noncentrosymmetric materials that host two spin-split Fermi surfaces with identical spin textures due to a spin-orbital intertwined effect. Incorporating multi-orbital repulsive Hubbard interactions, we calculate the superconducting pairings of a minimal two-orbital effective model within a spin-fluctuation-mediated superconductivity framework. We find that, depending on the effective Rashba spin-orbit coupling (RSOC) strength and filling level, the Hubbard interaction can drive the leading pairing symmetry into the  $A_1(S_{\pm})$ ,  $B_1$ ,  $B_2$  or  $B_2(d_{\pm})$  irreducible representations (IRs) of the  $C_{4v}$  point group. Notably, the  $A_1(S_{\pm})$  pairing gives rise to a fully gapped TSC characterized by a  $Z_2$  invariant, while the  $B_2(d_{\pm})$  pairing results in a nodal TSC. Our analysis reveals that the fully gapped TSC is predominated by spin-singlet regardless of the presence of the spin-triplet components. This distinguishes our model from non-centrosymmetric materials with conventional Rashba-split band structures, where TSC typically emerges near the van Hove singularity and is primarily driven by  $p$ -wave or  $f$ -wave spin-triplet pairing. These features enhances its experimental accessibility, and we discuss potential experimental systems for its realization.

*Introduction.*— TSCs can host Majorana bound states, which are exotic quasi-particles obeying non-Abelian statistics. This unique feature makes TSCs fundamentally fascinating and potentially valuable for applications in quantum computing[1–9]. Over the past two decades, many efforts have been devoted to realizing TSCs in various material platforms[10–18]. The general strategy involves utilizing superconducting proximity effects in either momentum space or real space. The former, also known as connate TSCs, is typically achieved in multiband superconducting systems with topological boundary states, such as Fe(Se,Te), PbTaSe<sub>2</sub> etc[13–20]. The latter approach involves the artificial construction of topological insulator (or semiconductor)-superconductor heterostructures[10–12]. However, these material platforms pose experimental challenges, requiring high interface quality, a large induced superconducting gap, and precise control of the chemical potential.

Unlike proximity-effect-induced TSCs, intrinsic TSCs exhibit topological properties throughout their entire volume, making them robust against perturbations at boundaries or interfaces[1]. This characteristic provides a significant advantage, positioning intrinsic TSCs as strong candidates for building quantum computing platforms. The pairing symmetry in intrinsic TSCs is typically  $p$ -wave spin-triplet, which generally arises only in unconventional superconducting systems driven by non-electron-phonon coupling mechanisms, making such materials exceedingly rare in nature. Current candidates include uranium- and cerium-based heavy fermion compounds, such as UTe<sub>2</sub>, CePt<sub>3</sub>Si[21–25]. Consequently, the exploration of new material systems for realizing

TSCs remains an important and active area of research.

A comprehensive analysis of material systems exhibiting TSC reveals that their Fermi surfaces typically form robust spin textures, indicating explicit or potential topological characteristics in their electronic structures. Notably, materials such as CePt<sub>3</sub>Si, Y<sub>2</sub>C<sub>3</sub>, A<sub>2</sub>Cr<sub>3</sub>As<sub>3</sub> (A=K, Rb, Cs)[24–29], which lack inversion symmetry, display similar features due to RSOC. Comparable spin texture characteristics have also been experimentally observed in the Fermi surfaces of certain copper- and iron-based superconducting systems[30, 31]. These insights suggest that TSCs may emerge in correlated unconventional superconducting systems when RSOC is considered. However, current research on single-orbital Rashba-Hubbard models indicates that the small contribution of the spin-triplet component in these systems is typically insufficient to realize TSCs, except under specific conditions, such as fillings close to the van Hove singularity[32–35].

To overcome the difficulties in realizing intrinsic TSCs, we propose an alternative approach by introducing a new degree of freedom, such as orbital, layer, or valley. For clarity, we focus on orbital degrees of freedom and consider a two-orbital Rashba-Hubbard model defined on a square lattice. Using the random phase approximation (RPA), we solve the superconducting problem of this model within the framework of spin-fluctuation-mediated superconductivity. We find that as the model parameters vary, the leading superconducting pairing can fall into the  $A_1(S_{\pm})$ ,  $B_1$ ,  $B_2$  or  $B_2(d_{\pm})$  of  $C_{4v}$  point group. Interestingly, the  $A_1(S_{\pm})$  pairing induces a sign-change gap function on the two Fermi surfaces with identical spin

textures. This sign-change feature is primarily driven by the spin-singlet-pairing components regardless of the presence of the spin-triplet components. Meanwhile, the  $A_1(S_{\pm})$  pairing leads to full-gap TSC states characterized by the topological invariant  $Z_2$ . This TSC is extraordinary and different from the ones driven by predominated  $p$ -wave or  $f$ -wave spin-triplet pairing. Additionally, the  $B_2(d_{\pm})$  pairing results in a nodal TSC state with coexistence of zero-energy flat-band and dispersive Majorana states at the system's boundary.

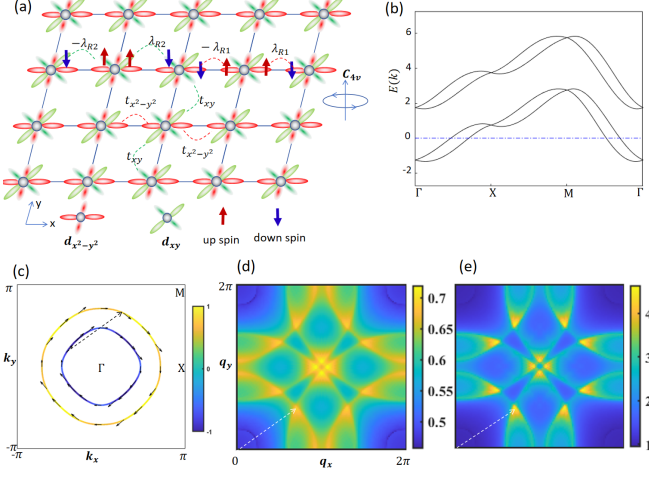


FIG. 1. (a) The two-orbital ( $d_{x^2-y^2}, d_{xy}$ ) unconventional Rashba model defined on a square lattice with  $C_{4v}$  symmetry. The relations between the parameters here and those in Eq. 2 are  $t_{1/2} = (t_{x^2-y^2} \pm t_{xy})/2$  and  $\lambda_R = (\lambda_{R1} + \lambda_{R2})/2$ . (b)-(c) The representative band structure and Fermi surfaces for electron doping. The black arrows on the Fermi surfaces denote the effective spin and the color bar labels the renormalized orbital texture  $\langle FS | \tau^z \sigma^0 | FS \rangle_k / \langle FS | \tau^z \sigma^0 | FS \rangle_{max}$ . The parameters  $t_2 = 0$ ,  $\lambda_R = 0.8$ ,  $\epsilon = 1$  and  $\mu = -4.5$ . (d-e) The calculated bare and RPA longitudinal spin susceptibilities  $\chi_0^{zz}(\mathbf{q})$  and  $\chi_{RPA}^{zz}(\mathbf{q})$ . The transverse parts are weak[43]. The parameters  $U = 4.5, V = 0.94U$  and  $J = 0.03U$ . Other parameters are the same as those in (b) and (c).

**Model and method.**— The two-orbital unconventional Rashba-Hubbard model is given by

$$H = H_0 + H_{int}, \quad (1)$$

with

$$H_0 = \sum_k \xi(k) - \lambda_R(\tau^0 + \epsilon\tau^3)[\boldsymbol{\sigma} \times \nabla_{\mathbf{k}}\gamma(k)]_z + \lambda\tau^2\sigma^3 \quad (2)$$

and

$$\begin{aligned} H_{int} = & U \sum_{i\alpha} \hat{n}_{i\alpha\uparrow} \hat{n}_{i\alpha\downarrow} + V \sum_{i\alpha < \beta} \sum_{\sigma\sigma'} \hat{n}_{i\alpha\sigma} \hat{n}_{i\beta\sigma'} \\ & - J \sum_{i,\alpha < \beta} \mathbf{S}_{i\alpha} \cdot \mathbf{S}_{i\beta} \\ & + J' \sum_{i,\alpha < \beta} \sum_{\sigma} c_{i\alpha\sigma}^\dagger c_{i\alpha\bar{\sigma}}^\dagger c_{i\beta\bar{\sigma}} c_{i\beta\sigma} \end{aligned} \quad (3)$$

Here,  $H_0$  can be defined on a lattice with the symmetry of  $C_{3v}$ ,  $C_{4v}$  or  $C_{6v}$ [36–38]. For clarity and simplicity, we consider square lattice with  $C_{4v}$ , as shown in Fig. 1 (a). The two orbital are fixed to be  $d_{x^2-y^2}$  and  $d_{xy}$ . Then,  $\xi(k) = 2(t_1\tau^0 + t_2\tau^3)\gamma(k) - \mu$  with  $\gamma(k) = \cos k_x + \cos k_y$  and  $\mu$  denoting the chemical potential.  $\lambda_R$  represents the strength of effective RSOC, and a parameter  $\epsilon$  is introduced to measure the anisotropy of two orbitals[39].  $\lambda$  is the strength of on-site SOC. To match the parameter settings in Fig. 1 (a),  $t_{1/2} = (t_{x^2-y^2} \pm t_{xy})/2$  and  $\lambda_R = (\lambda_{R1} + \lambda_{R2})/2$ . In the following,  $t_1$  is set to  $-1$ , and other parameters are in unit of  $|t_1|$ .  $\lambda$  is set to 3 throughout the calculations. Pauli matrices  $(\tau^0, \boldsymbol{\tau})$  and  $(\sigma^0, \boldsymbol{\sigma})$  span in orbital and spin spaces, respectively. Then,  $H_0$  spans in the basis  $\Psi_k = (c_{x^2-y^2,k,\uparrow}, c_{x^2-y^2,k,\downarrow}, c_{xy,k,\uparrow}, c_{xy,k,\downarrow})^T$  with  $c_{\alpha k, \sigma}$  being the electron annihilation operator.  $U$ ,  $V$ ,  $J$  and  $J'$  represents the intra- and inter-orbital on-site repulsive Hubbard interactions, Hund's coupling, and the pairing hopping term, respectively.  $\hat{n}_{i\alpha\sigma}$  and  $\mathbf{S}_{i\alpha}$  denote the spin- $\sigma$  electron density operator and spin operator for electrons in orbital  $\alpha$  on  $i$  site, respectively. For clarity, we adopt the conventional notations  $J = J'$  and  $V = U - 2J$  in the following discussion.

The general bare susceptibility can be expressed as follows,

$$\begin{aligned} \chi_{l_3\sigma_3l_4\sigma_4}^{l_1\sigma_1l_2\sigma_2}(\mathbf{q}, i\nu_n) \\ = -T \sum_{\mathbf{k}, i\omega_n} G_{l_3\sigma_3l_1\sigma_1}(\mathbf{k}, i\omega_n) G_{l_2\sigma_2l_4\sigma_4}(\mathbf{k}, i\omega_n - i\nu_n), \end{aligned} \quad (4)$$

with the Matsubara Green function,

$$\hat{G}(\mathbf{k}, i\omega_n) = [i\omega_n - H_0(\mathbf{k})]^{-1}. \quad (5)$$

Here,  $l_{1-4}$  are orbital index, and  $\sigma_{1-4}$  are spin index.  $i\omega_n$  and  $i\nu_n$  fermionic and bosonic Matsubara frequencies, respectively. Using RPA, the dressed susceptibility can be calculated by

$$\hat{\chi}^{RPA}(\mathbf{q}, i\nu_n) = [\hat{1} - \hat{\chi}(\mathbf{q}, i\nu_n)\hat{W}]^{-1}\hat{\chi}(\mathbf{q}, i\nu_n). \quad (6)$$

Here,  $\hat{W}$  is the bare interaction matrix with non-zero elements  $W_{l_1\sigma_1l_1\bar{\sigma}}^{l_1\sigma_1l_1\bar{\sigma}} = U$ ,  $W_{l_1\sigma_1l_1\bar{\sigma}}^{l_1\sigma_1l_1\sigma} = -U$ ,  $W_{l_2\sigma_1l_1\bar{\sigma}}^{l_2\sigma_1l_1\bar{\sigma}} = V$ ,  $W_{l_2\sigma_1l_1\bar{\sigma}}^{l_2\sigma_1l_1\sigma} = -V$ ,  $W_{l_2\sigma_2l_2\bar{\sigma}}^{l_2\sigma_2l_2\bar{\sigma}} = J$ ,  $W_{l_2\sigma_2l_2\bar{\sigma}}^{l_2\sigma_2l_2\sigma} = -J$ ,  $W_{l_1\sigma_1l_2\bar{\sigma}}^{l_1\sigma_1l_2\bar{\sigma}} = J'$ , and  $W_{l_2\sigma_1l_1\bar{\sigma}}^{l_1\sigma_1l_2\bar{\sigma}} = -J'$ .

According to the theory of fluctuation-mediated superconductivity[40–42], the effective static superconducting pairing interactions can be calculated by considering bubble and ladder diagrams[43], and are expressed as:

$$V_{l_3\sigma_3l_4\sigma_4}^{l_1\sigma_1l_2\sigma_2}(\mathbf{k}, \mathbf{k}') = W_{l_3\sigma_3l_4\sigma_4}^{l_1\sigma_1l_2\sigma_2} + V_l(\mathbf{k}, \mathbf{k}') - V_b(\mathbf{k}, \mathbf{k}'), \quad (7)$$

with the ladder term

$$V_l(\mathbf{k}, \mathbf{k}') = [\hat{W}\hat{\chi}^{RPA}\hat{W}]_{l_3\sigma_3l_4\sigma_4}^{l_1\sigma_1l_2\sigma_2}(\mathbf{k} + \mathbf{k}'), \quad (8)$$

and the bubble term

$$V_b(\mathbf{k}, \mathbf{k}') = [\hat{W} \hat{\chi}^{RPA} \hat{W}]_{l_3 \sigma_3 l_2 \sigma_2}^{l_1 \sigma_1 l_4 \sigma_4}(\mathbf{k} - \mathbf{k}'). \quad (9)$$

The possible superconducting pairing can be evaluated through solving the linear Eliashberg equation as follows,

$$\begin{aligned} \lambda \Delta_{l_1 \sigma_1 l_4 \sigma_4}(\mathbf{k}) \\ = T \sum_{\mathbf{k}' i \omega_n} \sum_{l_2 \sigma_2 l_3 \sigma_3} V_{l_3 \sigma_3 l_4 \sigma_4}^{l_1 \sigma_1 l_2 \sigma_2}(\mathbf{k}, \mathbf{k}') F_{l_3 \sigma_3 l_2 \sigma_2}(\mathbf{k}', i \omega_n), \end{aligned} \quad (10)$$

with

$$\begin{aligned} F_{l_3 \sigma_3 l_2 \sigma_2}(\mathbf{k}', i \omega_n) \\ = G_{l_3 \sigma_3 l \sigma}(\mathbf{k}', i \omega_n) \Delta_{l \sigma' l' \sigma'}(\mathbf{k}') G_{l_2 \sigma_2 l' \sigma'}(-\mathbf{k}', -i \omega_n). \end{aligned} \quad (11)$$

Here,  $\Delta_{l_1 \sigma_1 l_4 \sigma_4}(\mathbf{k})$  is the superconducting pairing function and the leading superconducting instability can be identified by the largest positive eigen-value of  $\lambda$ .

*Fermionology and spin susceptibility.*— Previous studies on the conventional Rashba-Hubbard model have focused on cases where the filling is near the van Hove singularity. This condition induces strong ferromagnetic fluctuations, which, in turn, favor the emergence of leading  $p$ - or  $f$ -wave spin-triplet superconducting states[32, 34, 35]. In this work, we relax this restriction and consider more general cases of electron doping beyond the van Hove singularity. Note that the hole doping is the mirror of the electron doping here. A typical band structure and Fermi surfaces under electron doping are shown in the Figs. 1 (b) and (c). Two Fermi surfaces have the same spin textures and apparent orbital textures, as shown in Fig. 1 (c).

The bare and RPA spin susceptibilities corresponding to the Fermi surfaces in Fig. 1 (c) can be calculated with Eqs. 4 and 6. The calculated results indicate that the transverse spin susceptibility  $\chi^{+-}(\mathbf{q})$  is consistently much smaller than the longitudinal spin susceptibility  $\chi^{zz}(\mathbf{q})$ [43]. Therefore, we focus on  $\chi^{zz}(\mathbf{q})$  as shown in Figs. 1 (d) and (e), which primarily determines the characteristics of spin fluctuations in the system. In both Figs. 1 (d) and (e), in addition to the four peaks near the  $(\pi, \pi)$ , eight new peaks emerge, as indicated by the white dashed arrows in these panels. These new peaks correspond to the nesting wave vectors of the two spin-split Fermi surfaces, which are consistent with the black dashed arrows shown in Fig. 1(a). This suggests that these eight new peaks play a crucial role in determining the characteristics of the potential superconducting state, distinguishing it from the single-orbital case. We also calculated the spin susceptibility for other doping cases[43] and found significantly different characteristics compared to the single orbital cases.

*Phase diagram and sign-change SC states.*— Once superconductivity is induced by antiferromagnetic fluctuations, the pairing symmetry of the superconducting state

TABLE I. Possible IRs of superconducting pairings under the constraints of group  $C_{4v}$ . Here,  $g_k = \sin k_x \sin k_y$ .

Pairing form	$\phi_{g/u} / \mathbf{d}_{g/u}$	IRs
$i\phi_g \sigma^2 \tau^{0/3(1)}$	$1, \cos k_x + \cos k_y, \cos k_x \cos k_y$	$A_1(A_2)$
	$\cos k_x - \cos k_y$	$B_1(B_2)$
	$\sin k_x \sin k_y$	$B_2(B_1)$
$i\phi_u \sigma^2 \tau^2$	$\{\sin k_x, \sin k_y\}$	$E$
$i(\mathbf{d}_u \cdot \boldsymbol{\sigma}) \sigma^2 \tau^{0/3(1)}$	$(-\sin k_y, \sin k_x, 0)$	$A_1(A_2)$
	$(\sin k_x, \sin k_y, 0)$	$A_2(A_1)$
	$(\sin k_y, \sin k_x, 0)$	$B_1(B_2)$
	$(\sin k_x, -\sin k_y, 0)$	$B_2(B_1)$
	$[(0, 0, \sin k_x), (0, 0, \sin k_y)]$	$E$
$i(\mathbf{d}_g \cdot \boldsymbol{\sigma}) \sigma^2 \tau^2$	$(0, 0, \cos k_x + \cos k_y)$	$A_1$
	$(0, 0, \cos k_x - \cos k_y)$	$B_1$
	$(0, 0, g_k)$	$B_2$
	$\{(\cos k_x/y, 0, 0), (0, \cos k_y/x, 0)\}$	$E$
	$\{(g_k, 0, 0), (0, g_k, 0)\}$	$E$

can be classified according to the IRs of the  $C_{4v}$  group. Table I lists the possible pairings with their form factors up to the next-nearest neighbor and their corresponding IRs. By solving the linear gap equation in Eq. (10), the leading superconducting pairing can be determined.

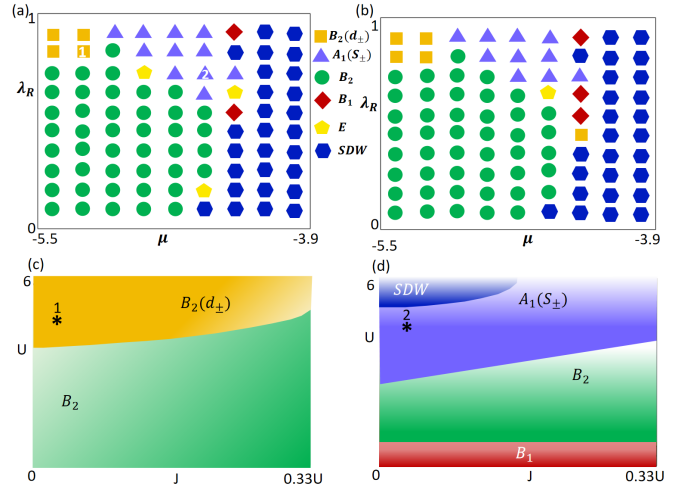


FIG. 2. The phase diagrams of superconducting states as functions of some parameters. (a)-(b)  $\lambda_R$ - $\mu$  phase diagram.  $U = 4.5$  and  $J = 0.03U$  in (a).  $U = 5.4$  and  $J = 0.21U$  in (b). (c)-(d)  $U$ - $J$  phase diagram.  $\lambda_R = 0.9$  and  $\mu = -5.3$  in (c).  $\lambda_R = 0.8$  and  $\mu = -4.5$  in (d). In (a)-(d), all other parameters are the same as those in Fig. 1 (b). In panel (a), the positions marked by numbers 1 and 2 correspond to the star-marked positions labeled 1 and 2 in (c) and (d). The notation  $S_{\pm}$  and  $B_{\pm}$  in  $A_1$  and  $B_2$  indicates that the superconducting gap functions on the two spin-split Fermi surfaces have opposite signs along the radial direction.

The phase diagrams of the superconducting state with respect to  $\lambda_R$ - $\mu$  and  $U$ - $J$  are shown in Figs. 2 and Figs. S4 and S6[43]. Over a wide-range parameter space, we identify three possible leading pairing channels:  $A_1$ ,

$B_1$ , and  $B_2$ . Notably, the superconducting states in the  $A_1$  and  $B_2$  channels exhibit highly unconventional sign-changing gap structures  $A_1(S_{\pm})$  and  $B_2(d_{\pm})$ , which indicate that the superconducting gap functions on the two spin-split Fermi surfaces have opposite signs along the radial direction as shown in Fig. 3 (a) and Fig. S9 (a)[43].

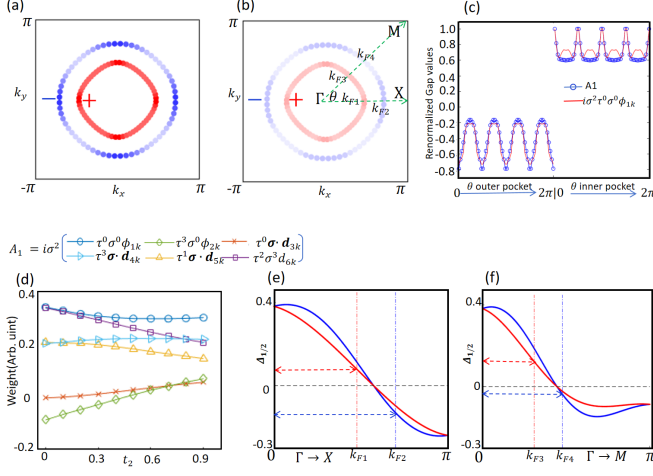


FIG. 3. (a)-(d) The superconducting gap functions projected onto the corresponding Fermi surfaces. The red and blue colors indicate the opposite signs of superconducting gap functions. (a) and (b) correspond to full and  $A_{1,1} = i\sigma^2\tau^0\sigma^0\phi_{1k}$  channels in  $A_1(S_{\pm})$  IR, respectively. (c) The renormalized gap function  $\Delta_{A_1}(k_F, \theta)/\max(\Delta_{A_1}(k_F, \theta))$  and  $\Delta_{A_{1,1}}(k_F, \theta)/\max(\Delta_{A_{1,1}}(k_F, \theta))$ . (d) The weights of six sub-channels in  $A_1(S_{\pm})$  IR as function as  $t_2$ . (e)-(f) The fitting gap function  $\Delta_{1/2}(k)$  in Eq. 13 along different high-symmetry lines  $\Gamma - M$  and  $\Gamma - X$ . Other parameters in (a)-(d) are the same as those in Fig. 1 (c) and of star labeled 2 in Fig. 2 (a) and (d).

To elucidate the origin of this unconventional sign-change superconducting state, we take the  $A_1(S_{\pm})$  channel as an example. The gap function of noncentrosymmetric systems can be parameterized as follows[44],

$$\hat{\Delta}_k = [\hat{\phi}_k + \hat{\mathbf{d}}_k \cdot \boldsymbol{\sigma}]i\sigma^2. \quad (12)$$

In the one-orbital Rashba model, the projection of the gap function onto the two spin-split Fermi surfaces can be expressed in a simplified form,  $\Delta_{1/2}(k) = \phi_k \pm |\hat{\mathbf{d}}_k|$  with  $\phi_k$  as a scalar. Thus, the aforementioned sign-change gap structure only occur when the triplet component is relatively strong and has helical  $p$ - or  $f$ -wave spin-triplet pairing, such as when the filling is near the van Hove singularity[32, 34, 35]. Any doping away from the van Hove singularity consistently results in predominant d-wave spin-singlet pairing[33]. However, for the two-orbital model considered here, additional possibilities arise. We project the six sub-channels  $i\sigma^2(\tau^0\sigma^0\phi_{1k}, \tau^3\sigma^0\phi_{2k}, \tau^0\boldsymbol{\sigma} \cdot \mathbf{d}_{3k}, \tau^3\boldsymbol{\sigma} \cdot \mathbf{d}_{4k}, \tau^1\boldsymbol{\sigma} \cdot \mathbf{d}_{5k}, \tau^2\sigma^3\phi_{6k})$  in the spin-orbital representation, listed in Table I onto the two Fermi surfaces. Note that the first two sub-channels

belong to spin-singlet while the latter four correspond to spin-triplet. The projection of the first sub-channel  $i\sigma^2\tau^0\sigma^0\phi_{1k}$  is shown in Fig. 3 (b), while the others are presented in Fig. S7 [43]. We find that their superconducting gap functions exhibit the same projected distribution on the Fermi surfaces, ensuring consistency with the overall superconducting gap projection, as illustrated in Figs. 3 (a), (b) and (c).

To further clarify the relative contributions of these six sub-channels to the overall sign-changing gap, we plot their contribution weights as a function of  $t_2$  in Fig. 3(d). We find that the first sub-channel  $i\sigma^2\tau^0\sigma^0\phi_{1k}$  consistently dominates as  $t_2$  increasing. In other words, the intra-orbital spin-singlet pairing always predominate the gap structure regardless of the presence of the spin-triplet pairings. Then, in the spin-orbital representation, the superconducting gap function in Eq. 12 can be approximated as  $\hat{\Delta}_k \sim i\sigma^2\tau^0\sigma^0\phi_{1k}$ . Considering up to the next-nearest-neighbor terms,  $\phi_{1k}$  can be fitted as  $-0.018 + 0.046(\cos k_x + \cos k_y) + 0.076\cos k_x \cos k_y$ . Consequently, in the band representation, the gap functions on the two Fermi surfaces can be expressed as

$$\Delta_{1/2}(k) = \sqrt{2(1 + |B_{\mathbf{k}}^{\pm}|^2)}\phi_{1k}, \quad (13)$$

with  $B_{\mathbf{k}}^{\pm} = i(\sqrt{\lambda^2 + h_{\mathbf{k}}^2\lambda_R^2} \pm \lambda_R h_{\mathbf{k}})/\lambda$  and  $h_{\mathbf{k}} = \sqrt{\sin^2 k_x + \sin^2 k_y}$ . In Fig. 3 (e) and (f), we plot  $\Delta_{1/2}(k)$  along the  $\Gamma - X$  and  $\Gamma - M$  directions, respectively. The sign-change feature of the gap function at the two Fermi momenta is clearly visible. Such sign-change gap structure is consistent with the Fermi surface nesting and  $\chi^{zz}(\mathbf{q})$  in Figs. 1 (c)-(e). Similar analysis can be performed for channel  $B_2(d_{\pm})$ , as shown in Figs. S8-S10[43]. The results indicate that its sign-change feature cannot come from the pure spin-singlet channel and depends on the mixing of spin-singlet and spin-triplet components[43], in contrast to the  $A_1(S_{\pm})$  pairing.

**Topological superconductivity**— For noncentrosymmetric systems with time-reversal symmetry, the criteria for identifying TSC require that a pair of spin-split Fermi surfaces enclose an odd number of time-reversal invariant momentum points, and the order parameter must have opposite signs on the two Fermi surfaces[45]. Additionally, the fully gapped superconducting state is preferable. According to this criterion, the Fermi surface in Fig. 1 (c) and the corresponding superconducting gap in Fig. 3 (a) or (b) support TSC.

For the two-dimensional system with time-reversal symmetry considered here, the Chern number is always zero, and the topological nature of the superconducting state can be characterized by a topological invariant  $Z_2$ . Due to the lack of spatial inversion symmetry, the  $Z_2$  invariant can be determined by calculating the Wannier centers of the superconducting state's wave functions[43, 46] and verified through the computation of



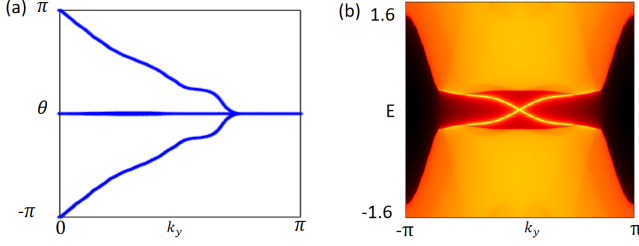


FIG. 4. (a) The Wilson loop calculation for the  $A_1(S_{\pm})$  superconducting state. (b) The quasi-particle spectrum of  $A_1(S_{\pm})$  superconducting state. Note that the in-gap edge states are double-degeneracy with opposite chirality. Periodic and open boundary conditions are applied along  $x$  and  $y$  direction, respectively. In both (a) and (b), the parameters are the same as those in Fig. 3 (a).

the edge spectrum[47, 48]. Figs. 4 (a) and (b) show the the Wannier center and edge spectrum, respectively, for the superconducting state with the Fermi surface from Fig. 1 (c) and the gap structure from Fig. 3 (b). It is straightforward to conclude that this superconducting state has a topological invariant  $Z_2 = 1$ . The superconducting state in  $B_2(d_{\pm})$  channel has nodes, however, it is also topologically nontrivial[43, 49], and exhibits Majorana flat bands and dispersive Majorana states on edges.

*Outlook and conclusion*— The TSC state driven by predominant  $s$ -wave spin-singlet pairing in our study has significant implications. First, TSC states realized through  $p$ - or  $f$ -wave spin-triplet pairing are extremely rare in real material systems. In contrast, almost all reported superconductors exhibit  $s$ -wave spin-singlet pairing, including cuprate, iron-based, and nickelate high-temperature superconductors[50–52]. Second, the splitting of Fermi surfaces accompanied by spin-texture characteristics due to broken inversion symmetry has been experimentally reported in systems such as cuprate and iron-based superconductors[30, 31]. For instance, spin splitting induced by Rashba SOC could potentially be tuned via electric fields or other external controls. Our proposal offers a viable pathway to realize bulk topological superconductivity in high-temperature superconducting systems without relying on proximity effects. If achieved, this could greatly advance the exploration of topological quantum computing based on topological superconductivity.

In summary, we investigated superconductivity in a new class of correlated non-centrosymmetric systems. Using the theory of antiferromagnetic-fluctuation-mediated superconductivity, we identified four possible superconducting states  $A_1(S_{\pm})$ ,  $B_1$ ,  $B_2$  and  $B_2(d_{\pm})$  under different model parameters. all of which are predominantly driven by spin-singlet pairing with  $A_1$ ,  $B_1$  and  $B_2$  pairing symmetries. Notably, the superconducting state with  $A_1(S_{\pm})$  IR is predominantly driven by spin-singlet pairing and belongs to a bulk topological superconduct-

ing state characterized by a  $Z_2 = 1$  topological invariant. Our proposal is different from all present scenarios based on proximity effects and strong  $p$ - or  $f$ -wave spin-triplet pairing. We further highlighted the potential realization of such topological superconducting states in certain high-temperature superconductors, providing a new pathway for exploring next-generation high-temperature topological superconductors.

This work was financially supported by the National Key R&D Program of China (Grants No. 2022YFA1403200, No. 2024YFA1613200 and Grant No. 2023YFA1407300), National Natural Science Foundation of China (Grants No. 92265104, No. 12022413 and No. 12447103), the Basic Research Program of the Chinese Academy of Sciences Based on Major Scientific Infrastructures (Grant No. JZHKYPT-2021-08), the CA-SHIPS Director’s Fund (Grant No. BJPY2023A09), Anhui Provincial Major S&T Project(s202305a12020005), and the High Magnetic Field Laboratory of Anhui Province under Contract No. AHM-FX-2020-02.

---

\* These authors make equal contributions.

† xxwu@itp.ac.cn

‡ haon@hml.ac.cn

- [1] D. A. Ivanov, Non-abelian statistics of half-quantum vortices in p-wave superconductors, *Physical review letters* **86**, 268 (2001).
- [2] A. Y. Kitaev, Fault-tolerant quantum computation by anyons, *Annals of physics* **303**, 2 (2003).
- [3] A. Kitaev, Anyons in an exactly solved model and beyond, *Annals of Physics* **321**, 2 (2006).
- [4] C. Nayak, S. H. Simon, A. Stern, M. Freedman, and S. Das Sarma, Non-abelian anyons and topological quantum computation, *Reviews of Modern Physics* **80**, 1083 (2008).
- [5] J. Alicea, New directions in the pursuit of majorana fermions in solid state systems, *Reports on progress in physics* **75**, 076501 (2012).
- [6] S. R. Elliott and M. Franz, Colloquium: Majorana fermions in nuclear, particle, and solid-state physics, *Reviews of Modern Physics* **87**, 137 (2015).
- [7] M. Z. Hasan and C. L. Kane, Colloquium: Topological insulators, *Rev. Mod. Phys.* **82**, 3045 (2010).
- [8] X.-L. Qi and S.-C. Zhang, Topological insulators and superconductors, *Rev. Mod. Phys.* **83**, 1057 (2011).
- [9] N. Read and D. Green, Paired states of fermions in two dimensions with breaking of parity and time-reversal symmetries and the fractional quantum hall effect, *Phys. Rev. B* **61**, 10267 (2000).
- [10] L. Fu and C. L. Kane, Superconducting proximity effect and majorana fermions? format?; at the surface of a topological insulator, *Physical review letters* **100**, 096407 (2008).
- [11] J. D. Sau, R. M. Lutchyn, S. Tewari, and S. Das Sarma, Generic new platform for topological quantum computation using semiconductor heterostructures, *Physical review letters* **104**, 040502 (2010).
- [12] S. Nadj-Perge, I. K. Drozdov, J. Li, H. Chen, S. Jeon,

- J. Seo, A. H. MacDonald, B. A. Bernevig, and A. Yazdani, Observation of majorana fermions in ferromagnetic atomic chains on a superconductor, *Science* **346**, 602 (2014).
- [13] N. Hao and J. Hu, Topological phases in the single-layer fese, *Physical Review X* **4**, 031053 (2014).
- [14] Z. Wang, P. Zhang, G. Xu, L. Zeng, H. Miao, X. Xu, T. Qian, H. Weng, P. Richard, A. V. Fedorov, *et al.*, Topological nature of the fese 0.5 te 0.5 superconductor, *Physical Review B* **92**, 115119 (2015).
- [15] X. Wu, S. Qin, Y. Liang, H. Fan, and J. Hu, Topological characters in fe (te 1- x se x) thin films, *Physical Review B* **93**, 115129 (2016).
- [16] N. Hao and J. Hu, Topological quantum states of matter in iron-based superconductors: from concept to material realization, *National Science Review* **6**, 213 (2019).
- [17] X. Wu, S. Qin, Y. Liang, C. Le, H. Fan, and J. Hu, Cafeas 2: A staggered intercalation of quantum spin hall and high-temperature superconductivity, *Physical Review B* **91**, 081111 (2015).
- [18] G. Xu, B. Lian, P. Tang, X.-L. Qi, and S.-C. Zhang, Topological superconductivity on the surface of fe-based superconductors, *Physical review letters* **117**, 047001 (2016).
- [19] T.-R. Chang, P.-J. Chen, G. Bian, S.-M. Huang, H. Zheng, T. Neupert, R. Sankar, S.-Y. Xu, I. Belopolski, G. Chang, *et al.*, Topological dirac surface states and superconducting pairing correlations in pbtase 2, *Physical Review B* **93**, 245130 (2016).
- [20] S.-Y. Guan, P.-J. Chen, M.-W. Chu, R. Sankar, F. Chou, H.-T. Jeng, C.-S. Chang, and T.-M. Chuang, Superconducting topological surface states in the noncentrosymmetric bulk superconductor pbtase2, *Science advances* **2**, e1600894 (2016).
- [21] L. Jiao, S. Howard, S. Ran, Z. Wang, J. O. Rodriguez, M. Sigrist, Z. Wang, N. P. Butch, and V. Madhavan, Chiral superconductivity in heavy-fermion metal ute2, *Nature* **579**, 523 (2020).
- [22] D. Aoki, A. Nakamura, F. Honda, D. Li, Y. Homma, Y. Shimizu, Y. J. Sato, G. Knebel, J.-P. Brison, A. Pourret, *et al.*, Unconventional superconductivity in heavy fermion ute2, *journal of the physical society of japan* **88**, 043702 (2019).
- [23] D. Aoki, J.-P. Brison, J. Flouquet, K. Ishida, G. Knebel, Y. Tokunaga, and Y. Yanase, Unconventional superconductivity in ute2, *Journal of Physics: Condensed Matter* **34**, 243002 (2022).
- [24] E. Bauer, G. Hilscher, H. Michor, C. Paul, E.-W. Scheidt, A. Gribanov, Y. Seropegin, H. Noël, M. Sigrist, and P. Rogl, Heavy fermion superconductivity and magnetic order in noncentrosymmetric c e p t 3 s i, *Physical review letters* **92**, 027003 (2004).
- [25] M. Smidman, M. Salamon, H. Yuan, and D. Agterberg, Superconductivity and spin-orbit coupling in non-centrosymmetric materials: a review, *Reports on Progress in Physics* **80**, 036501 (2017).
- [26] M. Krupka, A. Giorgi, N. Krikorian, and E. Szklarz, High pressure synthesis and superconducting properties of yttrium sesquicarbide, *Journal of the Less Common Metals* **17**, 91 (1969).
- [27] J.-K. Bao, J.-Y. Liu, C.-W. Ma, Z.-H. Meng, Z.-T. Tang, Y.-L. Sun, H.-F. Zhai, H. Jiang, H. Bai, C.-M. Feng, *et al.*, Superconductivity in quasi-one-dimensional k 2 cr 3 as 3 with significant electron correlations, *Physical Review X* **5**, 011013 (2015).
- [28] Z.-T. Tang, J.-K. Bao, Y. Liu, Y.-L. Sun, A. Ablimit, H.-F. Zhai, H. Jiang, C.-M. Feng, Z.-A. Xu, and G.-H. Cao, Unconventional superconductivity in quasi-one-dimensional rb 2 cr 3 as 3, *Physical Review B* **91**, 020506 (2015).
- [29] Z.-T. Tang, J.-K. Bao, Z. Wang, H. Bai, H. Jiang, Y. Liu, H.-F. Zhai, C.-M. Feng, Z.-A. Xu, and G.-H. Cao, Superconductivity in quasi-one-dimensional cs 2 cr 3 as 3 with large interchain distance, *Science China Materials* **58**, 16 (2015).
- [30] K. Gotlieb, C.-Y. Lin, M. Serbyn, W. Zhang, C. L. Smallwood, C. Jozwiak, H. Eisaki, Z. Hussain, A. Vishwanath, and A. Lanzara, Revealing hidden spin-momentum locking in a high-temperature cuprate superconductor, *Science* **362**, 1271 (2018).
- [31] S. Borisenko, D. Evtushinsky, Z.-H. Liu, I. Morozov, R. Kappenberger, S. Wurmehl, B. Büchner, A. Yaresko, T. Kim, M. Hoesch, *et al.*, Direct observation of spin-orbit coupling in iron-based superconductors, *Nature Physics* **12**, 311 (2016).
- [32] A. Greco and A. P. Schnyder, Mechanism for unconventional superconductivity in the hole-doped rashba-hubbard model, *Physical Review Letters* **120**, 177002 (2018).
- [33] K. Nogaki and Y. Yanase, Strongly parity-mixed superconductivity in the rashba-hubbard model, *Physical Review B* **102**, 165114 (2020).
- [34] A. Greco, M. Bejas, and A. P. Schnyder, Ferromagnetic fluctuations in the rashba-hubbard model, *Physical Review B* **101**, 174420 (2020).
- [35] P. M. Bonetti, D. Chakraborty, X. Wu, and A. P. Schnyder, Interaction-driven first-order and higher-order topological superconductivity, *Physical Review B* **109**, L180509 (2024).
- [36] X. Huang, Y. Xiao, R. Song, and N. Hao, Generic model with unconventional rashba bands and giant spin galvanic effect, *Physical Review B* **109**, 195419 (2024).
- [37] R. Wang, J. Li, X. Huang, L. Wang, R. Song, and N. Hao, Superconductivity in two-dimensional systems with unconventional rashba bands, *Physical Review B* **110**, 134517 (2024).
- [38] R. Wang, S.-B. Zhang, and N. Hao, Finite-momentum pairing state in unconventional rashba systems, *Physical Review B* **111**, L100506 (2025).
- [39] Here, we use anisotropic intra-orbital  $\tau^3$  term to replace the inter-orbital  $\tau^1$  term used in refs. [36–38]. note that these two cases are equivalent and can transform in to each other through an unitary operator  $(\tau^0 + i\tau^2)/\sqrt{2}$ . here, for convenience to define the model on square lattice, we adopt the former case, .
- [40] N. Berk and J. Schrieffer, Effect of ferromagnetic spin correlations on superconductivity, *Physical Review Letters* **17**, 433 (1966).
- [41] V. Emery, Theories of liquid helium three, *Annals of Physics* **28**, 1 (1964).
- [42] D. J. Scalapino, A common thread: The pairing interaction for unconventional superconductors, *Reviews of Modern Physics* **84**, 1383 (2012).
- [43] Supplementary materials including the detials of rpa, the effect of interorbital interaction, and gap functions, .
- [44] L. P. Gor'kov and E. I. Rashba, Superconducting 2d system with lifted spin degeneracy: mixed singlet-triplet state, *Physical Review Letters* **87**, 037004 (2001).

- [45] X.-L. Qi, T. L. Hughes, and S.-C. Zhang, Topological invariants for the fermi surface of a time-reversal-invariant superconductor, *Physical Review B—Condensed Matter and Materials Physics* **81**, 134508 (2010).
- [46] R. Yu, X. L. Qi, A. Bernevig, Z. Fang, and X. Dai, Equivalent expression of  $\mathbb{Z}_2$  topological invariant for band insulators using the non-abelian berry connection, *Physical Review B—Condensed Matter and Materials Physics* **84**, 075119 (2011).
- [47] N. Hao, P. Zhang, Z. Wang, W. Zhang, and Y. Wang, Topological edge states and quantum hall effect in the haldane model, *Physical Review B—Condensed Matter and Materials Physics* **78**, 075438 (2008).
- [48] N. Hao, P. Zhang, and Y. Wang, Topological phases and fractional excitations of the exciton condensate in a special class of bilayer systems, *Physical Review B—Condensed Matter and Materials Physics* **84**, 155447 (2011).
- [49] M. Sato, Y. Tanaka, K. Yada, and T. Yokoyama, Topology of andreev bound states with flat dispersion, *Physical Review B—Condensed Matter and Materials Physics* **83**, 224511 (2011).
- [50] J. G. Bednorz and K. A. Müller, Possible high  $T_c$  superconductivity in the  $\text{Ba-La-Cu-O}$  system, *Zeitschrift für Physik B Condensed Matter* **64**, 189 (1986).
- [51] Y. Kamihara, T. Watanabe, M. Hirano, and H. Hosono, Iron-based layered superconductor  $\text{La}_{1-x}\text{Fe}_x\text{FeAs}$  ( $x=0.05-0.12$ ) with  $T_c=26$  K, *Journal of the American Chemical Society* **130**, 3296 (2008).
- [52] H. Sun, M. Huo, X. Hu, J. Li, Z. Liu, Y. Han, L. Tang, Z. Mao, P. Yang, B. Wang, *et al.*, Signatures of superconductivity near 80 K in a nickelate under high pressure, *Nature* **621**, 493 (2023).